Approved for 26 days with A-

Precision Measurement of Longitudinal and Transverse Response Functions of Quasi-Elastic Electron Scattering in the Momentum Transfer Range $0.55\ \mathrm{GeV}/c \leq |\mathbf{q}| \leq 1.0\ \mathrm{GeV}/c$

J. Morgenstern
CEA Saclay DSM/DAPNIA/SPhN F91191, Gif-sur-Yvette Cedex, France

J. Templon
University of Georgia, Athens, GA 30602

J.-P. Chen (Co-spokesperson), E. Chudakov, C. W. de Jager, M. Jones, J. Gomez, J.-O. Hansen, J. LeRose, N. Liyanage, R. Michaels, J. Mitchell, A. Saha, B. Wojtsekhowski
Jefferson Lab, Newport News, VA 23606

A.T Katramatou, K. McCormick, G.G. Petratos
Kent State University, Kent, OH 44242

W. Korsch, P. Zolnierczuk
University of Kentucky, Lexington, KY 40506

W. Bertozzi, S. Gilad, D.W. Higinbotham, S. Sirca, R. Suleiman, Z. Zhou
Massachusetts Institute of Technology, Cambridge, MA 02139, USA

F. Benmokhtar, S. Dieterich, R. Gilman, C. Glashausser, X. Jiang, G. Kumbartzki, R. Ransome, S. Strauch
Rutgers University, Piscataway, NJ 08855

Seonho Choi (Spokesperson), A. Lukhanin, Z.-E. Meziani (Co-spokesperson),
K. Slifer, P. Solvignon, J. Shousky
Temple University, Philadelphia, PA 19122

T. Averett
College of William and Mary, Williamsburg, VA 23185

and

Hall A Collaboration

Contact: Seonho Choi (choi@jlab.org)

February 5, 2001

Abstract

We propose to make a precision measurement of inclusive electron scattering cross sections in the quasi-elastic region for a wide range of momentum transfers for ^{4}He, ^{12}C, ^{56}Fe and ^{208}Pb. We will extract the longitudinal and transverse response functions in the momentum transfer range 0.55 GeV/$c \leq |\mathbf{q}| \leq$ 1.0 GeV/c with a precision of a few percent improving significantly on the precision of previous measurements in the overlap region. This should allow us to confirm/refute the presently controversial issue of the quenching of the longitudinal response function in medium weight nuclei and as importantly investigate the $|\mathbf{q}|$ evolution of the Coulomb Sum Rule as we probe significantly shorter distances.

1 Introduction and Motivation

One of the important questions in nuclear physics is how nucleon properties are affected by the nuclear medium, since it might form a bridge between the strong interaction between nucleons and the underlying theory of Quantum ChromoDynamics (QCD). A good example is the partial restoration of chiral symmetry in nuclear matter and its consequence for nucleon properties in the nuclear medium (for a comprehensive review see Ref. [1]). Since elastic scattering from a free nucleon has been well measured, quasi-elastic electron scattering off nuclei is considered a promising tool to investigate the properties of nucleons in nuclei. In particular, it was proposed [2] that a Rosenbluth separation of the charge and magnetic responses of a nucleus (R_L and R_T, respectively) could test a model-independent property known as the Coulomb sum rule (CSR). This sum rule states that when integrating the quasi-elastic $R_L(q,\omega)$ over the full range of energy loss ω at large enough three-momentum transfer $|\mathbf{q}| = q$ (greater than twice the Fermi momentum, $q \geq 500$ MeV/c), one should count the number of protons (Z) in a nucleus. More explicitly the quantity $S_L(q)$ defined by

$$S_L(q) = \frac{1}{Z}\int_{0^+}^{\infty} \frac{R_L(q,\omega)}{\tilde{G_E}^2} d\omega$$

is predicted to be unity in the limit of large q. Here $\tilde{G_E} = (G_E^p + N/ZG_E^n)\zeta$ takes into account the nucleon charge form factor inside the nucleus (which is usually taken to be equal to that of a free nucleon) as well as a relativistic correction (ζ) suggested by de Forest [3]. The lower limit of integration 0^+ excludes the elastic peak and the excited states of the nucleus.

This simple picture can be spoiled by the modification of the free nucleon electromagnetic properties by the nuclear medium and the presence of nucleon-nucleon short-range correlations. However, it is expected that around q of 500 MeV/c, S_L should not deviate more than a few percent from unity due to nucleon-nucleon correlations, and reach unity at higher q-values, independent of the nucleon-nucleon force chosen. Thus, a result of S_L far from unity might indicate a possible modification of the nucleon electric properties in the nuclear medium at moderate distances (for example a change in the pion cloud charge distribution) while at very short distances the nucleon hard core might remain unmodified. While there are several theoretical approaches (for example, see Ref. [4] and references therein) on

how to treat nucleons in nuclei the experimental situation is not ideal to help settle the important theoretical issues.

In the last twenty years a large experimental program has been carried out at Bates [5, 6, 7, 8, 9, 10, 11, 12], Saclay [13, 14, 15, 16, 17] and SLAC [18, 19] aimed at the extraction of R_L and R_T for a variety of nuclei. Overall consistency of the data set between different laboratories has been observed except for ^{40}Ca between Bates [12] and Saclay [14, 15].

At Bates and Saclay, Rosenbluth separations were only performed up to q of 550 MeV/c, because of the maximum beam energy limitations ($\sim$800 MeV/c), while at SLAC, only a measurement at q=1140 MeV/c was performed due to the minimum beam energy available ($\sim$900 MeV/c). In this respect, Jefferson Lab offers a unique opportunity to overlap and extend the world data on R_L and R_T with a significantly improved precision.

In the case of medium-weight and heavy nuclei conclusions reached by different experiments ranged from a full saturation of the CSR to its violation by 30 %. As a result a spectrum of explanations has emerged ranging from questioning the validity of the experiments (i.e., experimental backgrounds and inadequate Coulomb corrections especially for heavy nuclei) to suggesting a picture of a "swollen nucleon" in the nuclear medium due to a partial deconfinement [20, 21, 22, 23].

A recent analysis by Jourdan [24, 25] which included data from all laboratories and uses Coulomb corrections through a Local Effective Momentum Approximation (LEMA) calculation by the Ohio group [26], concluded that the data are consistent with the saturation of the Coulomb Sum Rule, $S_L(q = 570 \text{ MeV}/c) = 0.91 \pm 0.12$. The LEMA is supported by a full Distorted Wave Born Approximation (DWBA), however, it has been shown recently [27], by comparing quasi-elastic electron and positron scattering off ^{12}C and ^{208}Pb, that the Effective Momentum Approximation (EMA) can adequately describe quasi-elastic scattering, at variance with the LEMA calculations by the Ohio group [26].

We also point out that the error bar on S_L is underestimated because the systematic error contributions resulting from the use of several laboratory data are poorly known. Furthermore, at the q value chosen, extrapolations were necessary for R_L at the excitation energies in the dip region, leading to a larger uncertainty in the evaluation of systematic errors.

A global reanalysis of the existing data was undertaken by Morgenstern and Meziani (M&M) using the EMA to correct for the Coulomb corrections and Rosenbluth separations were performed to extract R_L and R_T for

Table 1: Comparison of the Coulomb Sum in ^{56}Fe, obtained by Jourdan and from the M&M analysis at $q = 570$ MeV/c. (*) No SLAC data were used in this case.

Analysis	Saclay Uncertainty	SLAC Uncertainty	Coulomb Correction	S_L
Jourdan	total	statistical	No	0.86±0.12
	total	statistical	Yes	0.91±0.12
M&M	total	(*)	No	0.72±0.23
	total	(*)	Yes	0.63±0.20
	total	total	No	0.82±0.12
	total	total	Yes	0.73±0.12

medium weight and heavy nuclei. The quantitative difference of the experimental Coulomb sum results between Jourdan analysis and M&M analysis [28] is summarized in Table 1. Two sources of difference are identified; (a) the Coulomb corrections and (b) the use of the total error in the Saclay data but only the statistical error in the SLAC data by Jourdan. For (a), the Coulomb corrections used in [24, 25] following the prescription of [26], at variance with the experimental confirmation of the EMA [27], have the opposite sign; they increase R_L instead of decreasing it. From Figs. 8 and 9 of Ref. [27] it is clear that these corrections reduce the magnitude of the large ω tail while in the case of [26] they enhance it: the Coulomb corrections of M&M reduce S_L by 10% while Jourdan's increase it by 5%. The reduction of R_L when using the EMA was already observed in the analysis of SLAC experiment NE9 [18]. For (b), more weight was given to the SLAC NE3 data by using only their statistical error in the Rosenbluth procedure leading to an artificial enhancement of R_L by 4%.

Figure 1 shows the results obtained for S_L of ^{40}Ca, ^{48}Ca, ^{56}Fe and ^{208}Pb in this new analysis[28]. In order to evaluate S_L the Simon [29] parametrization was used for the proton charge form factor, while for the neutron charge form factor the recent data by Herberg *et al.* [30] were taken into account. The results are compared to theoretical calculations for nuclear matter [31] (solid black curve) and ^{4}He [32] (dashed curve); the results in these two cases as expected are very similar and exhibit only a few percent quenching beyond

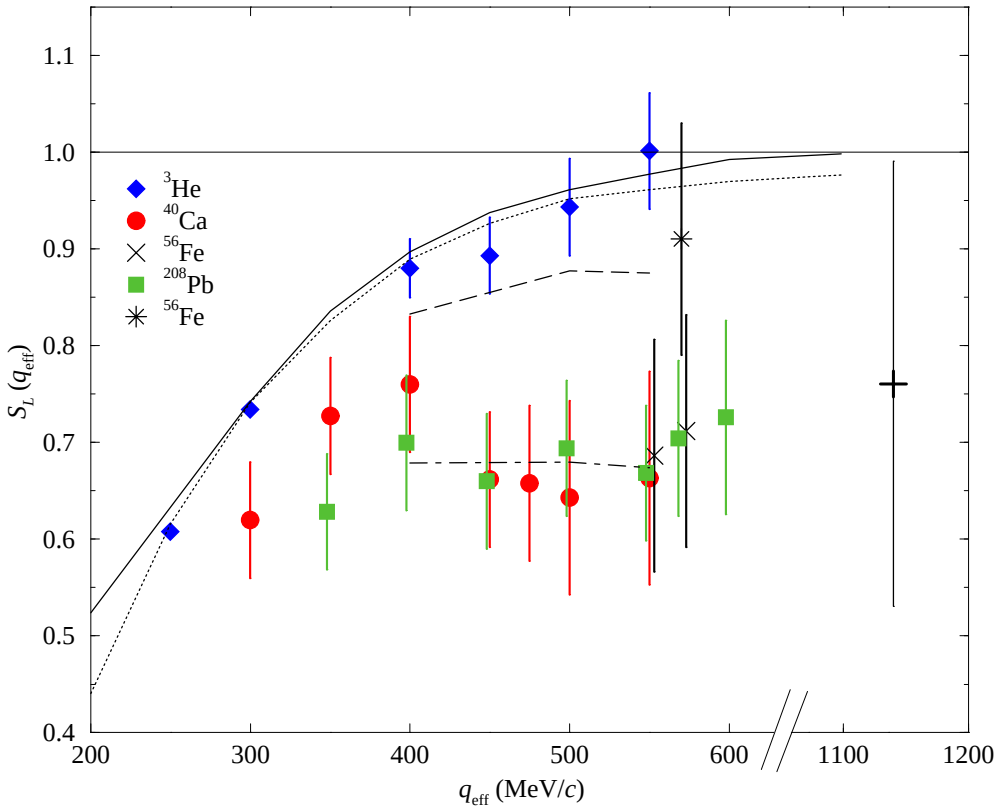

Figure 1: S_L obtained in the EMA as a function of q_{eff} using Saclay data combined with SLAC NE3 and Bates data. The ^{56}Fe SLAC NE9 result [18] (right cross) and that of the Jourdan analysis (star) are also shown. For the curves see the text.

$q_{eff} \sim 500$ MeV/c. The experimental results are to be compared with the long-dashed curve which corresponds to the same calculations as the solid curve but integrated within the experimental limits of excitation energy ω. A quenching of between 20% and 30% in medium weight nuclei persists.

While the interpretation of the results is still open to debate it is our aim in this proposal to provide for a significantly improved experimental data in a momentum transfer region mainly unexplored. There is one result at q = 1140 MeV/c from SLAC NE9 , but the experimental uncertainty leaves large room for constraining theoretical models of the Coulomb sum rule. Of course the momentum transfer range is chosen to overlap with previous measurements in order to settle the issue of the existence of quenching once

and for all but investigating the q evolution of R_L in a totally unchartered territory is also of paramount importance.

At Jefferson Lab, we can make a measurement with improved precision compared to the existing data. We propose to measure the evolution of the Coulomb sum between $q = 550$ MeV/c and $q = 1000$ MeV/c in order to verify/refute its quenching at moderate momentum transfer and to investigate its saturation at high momentum transfer. This measurement will be performed on several targets from ^{4}He to ^{208}Pb in order to address the issue of density dependence and Coulomb corrections. Whether the explanation of effects is from short range correlations or electromagnetic properties modifications, this new measurement will have a positive impact on our understanding of the behavior of nucleons in the nuclear medium.

2 Separation of R_L and R_T

Under the assumption of one-photon exchange, the differential cross section of the inclusive electron scattering can be written as follows:

$$\frac{d^3\sigma}{d\Omega d\omega} = \sigma_{\rm M}\left[\frac{Q^4}{\mathbf{q}^4}R_L(|\mathbf{q}|,\omega) + \frac{Q^2}{2\mathbf{q}^2}\frac{R_T(|\mathbf{q}|,\omega)}{\varepsilon}\right]$$

where

$$\varepsilon(|\mathbf{q}|,\omega,\theta) = \left[1 + \frac{2\mathbf{q}^2}{Q^2}\tan^2\frac{\theta}{2}\right]^{-1},$$

$Q^2 = \mathbf{q}^2 - \omega^2$ gives the four-momentum squared of the exchanged virtual photon, ε is its polarization parameter, ω is the energy loss of the scattered electron, θ its laboratory scattering angle, $\sigma_{\rm M}$ is the Mott cross section, and $R(|\mathbf{q}|,\omega,\theta)$ is the total response function.

In order to extract R_L and R_T, we need to measure the cross sections at a minimum of two different angles keeping $|\mathbf{q}|$ and ω constant. Let σ_f and σ_b be the cross sections measured at the forward (f) and backward (b) angles respectively. In the same way, let ε_f and ε_b be the two corresponding virtual photon polarizations. Then solving two simultaneous linear equations lead us to the following expressions for R_L and R_T:

$$R_L = \frac{|\mathbf{q}|^4}{Q^4\sigma_{\rm M}}\frac{1}{(\varepsilon_f - \varepsilon_b)}(\varepsilon_f\sigma_f - \varepsilon_b\sigma_b)$$

$$R_T = \frac{|\mathbf{q}|^2}{Q^2\sigma_{\rm M}}\frac{2\varepsilon_f\varepsilon_b}{(\varepsilon_f - \varepsilon_b)}(\sigma_b - \sigma_f)$$

The final goal of the measurement is to study the response functions at constant $|\mathbf{q}|$. However, keeping $|\mathbf{q}|$ constant is almost impractical since in Hall A, it involves continuous change of beam and scattered electron energies. Instead, at constant angle but various, discrete values of the beam energy, we can cover as much space as possible in the $(\mathbf{q}, \omega)$ domain by changing continuously the energy of the scattered electrons. Then, by using an appropriate interpolation method we can deduce the cross section at specific values of $(\mathbf{q}, \omega)$. Once forward and backward cross sections at specfic values of $(\mathbf{q}, \omega)$ have been determined, we use the Rosenbluth separation to extract R_L and R_T for each $(\mathbf{q}, \omega)$.

3 Kinematics

In order to minimize the uncertainty in R_L, it is important to measure the cross section at the largest and smallest ε possible (or the most forward and backward angle, respectively). For the most forward angle, we chose 15° although the spectrometers in Hall A can be moved a little more forward with the presence of technicians. Our choice is close enough to the most forward angle without overhead time for special handling.

For the backward angle, we need to find a compromise with rapidly dropping counting rates and the lowest detectable energy by the spectrometers. We also find 120° to be the largest angle practical given these constraints. This allows for the largest Rosenbluth lever arm within a single experiment compared to all previous experiments.

In order to perform a Rosenbluth separation, the minimum number of necessary angles is two. However, having additional angles enables us to check for any angle dependent systematic errors and the linearity of the Rosenbluth plot. We choose two more angles 60° and 90°, which gives us four ε approximately equally spaced.

To have as much coverage as possible in $(\mathbf{q}, \omega)$ to reduce systematic uncertainties in the interpolation procedure, we need beam energies ranging from 400 MeV to 4 GeV. For the most forward angle, the necessary beam energies range from 1.2 GeV to 4.0 GeV. For all the other angles, we need beam energies ranging from 0.4 GeV to 1.2 GeV. Taking data at various beam energies at four constant scattering angles has an added advantage of reducing systematic uncertainties in the radiative corrections procedure. Finally, the measurement at high ω requires spectrometer momentum settings

down to 100 MeV/c.

With this choice of kinematics, we can measure response functions from $|\mathbf{q}| = 550$MeV/c to 1000 MeV/c. At each $|\mathbf{q}|$, the excitation energy range covers the quasi-elastic peak and part of Δ-resonance where R_L is expected to be small or close to zero[33].

Figures 2 to 5 show the actual coverage in Q^2 and ω for each spectrometer momentum setting at the most forward and backward angles. In the figures, lines are drawn showing constant $|\mathbf{q}| = 550$ MeV/c and 1000 MeV/c and $W = 940$ MeV/c^2 and 1232 MeV/c^2. Table 5 lists all the kinematic settings.

4 Estimation of Accuracy of R_L and R_T

We can estimate the uncertainty in the extracted response functions due to the relative statistical uncertainty $\Delta\sigma/\sigma$, the lever arm $\Delta\varepsilon$ and the ratio σ_L/σ_T. The uncertainty is expressed as:

$$\begin{aligned}
\frac{\Delta R_L}{R_L} &= \frac{\Delta\sigma}{\sigma}\frac{1}{\Delta\varepsilon}\sqrt{\left(\frac{1}{R}+\varepsilon_f\right)^2+\left(\frac{1}{R}+\varepsilon_b\right)^2} \\
\frac{\Delta R_T}{R_T} &= \frac{\Delta\sigma}{\sigma}\frac{R}{\Delta\varepsilon}\sqrt{\varepsilon_f^2\left(\frac{1}{R}+\varepsilon_b\right)^2+\varepsilon_b^2\left(\frac{1}{R}+\varepsilon_f\right)^2}
\end{aligned}$$

In this expression, $R = \sigma_L/\sigma_T$ is the ratio of longitudinal and transverse virtual photo-absorption cross sections. From these two expressions, we note that the uncertainty in the extracted response functions is inversely proportional to $\Delta\varepsilon$. Figure 6 shows the difference of the virtual photon polarization ε between the forward and backward angle for a few values of $|\mathbf{q}|$. Typically, we can achieve $\Delta\varepsilon = \varepsilon_f - \varepsilon_b = 0.85$ compared to a typical $\Delta\varepsilon \simeq 0.5$ in the previous measurements. The increase in $\Delta\varepsilon$ achievable in Hall A of Jefferson Lab combined with low relative systematic uncertainties in the determination of beam energy, its position and scattering angle makes a crucial improvement in the uncertainties on the extraction of the response functions and therefore on the Coulomb Sum determination.

Using $R = \sigma_L/\sigma_T$ values for ^{56}Fe from [14, 15, 18] and assuming statistical uncertainty of 1% for each 10 MeV excitation energy bin, the statistical uncertainty of R_L at the quasi-elastic peak has been estimated for the two values of |q|. Figures 7 and 8 shows the comparison of expected statistical uncertainties at Jefferson Lab with the existing data. We can achieve more data points with better statistical precision.

5 Experiment

We propose to measure cross sections over the whole quasi-elastic scattering and part of the Δ resonance region on ^{4}He, ^{12}C, ^{56}Fe and ^{208}Pb at four different angles and 16 incident beam energies as a function of A and nuclear density.

5.1 Target

Our choice of targets ranging from ^{4}He to ^{208}Pb allows us to study any A or density dependent effect one might observe. Furthermore, Coulomb corrections can be addressed by the same targets since we expect small Coulomb corrections for ^{4}He and ^{12}C, but rather significant corrections for ^{208}Pb.

For ^{4}He target, we plan to use Hall-A Cryo target which provides ^{4}He gas at 15 atmospheres at 5.8K. The length of the target is 10 cm so the density is equal to 1.4 g/cm^2. Due to the short length of ^{4}He target, we also need to do a measurement on a dummy cell to measure the contribution from the cell windows. For the nuclei other than ^{4}He, solid targets of thickness 100 mg/cm^2 will be used. For ^{208}Pb, two different target thicknesses will be used to check the radiative corrections.

5.2 Beam Current

The trigger rate for each spectrometer is limited to 2 kHz and this limits the used beam current. With the new helium cooled ^{56}Fe and ^{208}Pb target in Hall A, we can use up to 50 μA without damage due to heat produced by energy loss of the beam in the target. For the ^{4}He gas target, we can use a much higher beam current, but to avoid too much change in target density at high beam current, we plan to use only 50 μA for maximum beam current. The beam will be rasterized to reduce localized heating and possible damage to the target.

5.3 Spectrometers

Since this experiment is not a coincidence measurement, the two spectrometers of Hall-A can do independent measurements at a given beam energy. We shall optimize the angle settings to minimize the overhead of momentum and angle changes.

6 Background Considerations

There are three major sources of contamination in the measured cross section: pions, electrons from γ rays and scattering of electrons inside the spectrometer. The pion cross section increases as the energy transfer ω to the nucleus increases. However, using the Čerenkov and the Pb-glass detectors of the Hall A spectrometers, we have achieved typical pion rejection ratio of 5000.

The lowest scattered electron energy we will detect is 100 MeV at the backward angles. At this low energy spectrometer setting, the contribution of electrons from (e^+, e^-) pairs created from γ rays by the bremsstrahlung of the beam or by the decay of π^0 produced in the target needs to be subtracted from the electron yields. By reversing the polarity of the spectrometer with the detection system unchanged, we can measure the positron yields from this process and subtract an equal amount from the electron yields assuming charge symmetry of the process.

The scattering of the electrons inside the spectrometer, such as pole tip scattering usually generates uniform background on the focal plane. In particular, the measured momentum via reconstructed tracks in the wire chamber does not correspond to the actual momentum of the particle. This type of contamination could be important especially at the backward angles where the reaction cross sections are small. We plan to study this type of background using the existing data from Hall A and our own Monte-Carlo simulation.

To eliminate this kind of contamination, it is most effective to use a customized collimator so that no particles accepted by the spectrometer will scatter on the matter inside of it. From the Monte-Carlo simulation, we can design and build a few different shapes for the collimator. To choose an optimal shape, we need additional beam time to measure the rates of the scattered electrons inside the spectrometer. Once the study is done, we can choose one of the customized collimators which will eliminate this type of background.

7 Systematic Errors

To estimate systematic errors, we start from the cross section expression:

$$\frac{d^3\sigma}{d\Omega d\omega} = \frac{N_{\rm detected}(1.0+\varepsilon_i)(1.0+{\rm DT})}{\left(\int \frac{\rho N_A}{A} dx\right)\left(\int \frac{I}{e} dt\right)\left(\int d\Omega d\omega\right)},$$

where

$$
\begin{aligned}
N_{\text{detected}} &= \text{Number of events detected} \\
\varepsilon_i &= \text{Inefficiency of the detector system} \\
\text{DT} &= \text{Dead Time} \\
\rho &= \text{Density of the target} \\
N_A &= \text{Avogadro Number}, 6.022 \times 10^{23} \\
A &= \text{Atomic number of the target} \\
I &= \text{Beam current} \\
e &= \text{Charge of the electron}, 1.602 \times 10^{-19}\text{C}
\end{aligned}
$$

- The uncertainty on the detector inefficiencies is less than 0.3%.
- There are two kinds of dead time corrections: one from the electronics and the other from the computer. The electronics dead time is less than 1%. The computer dead time can be as big as 10% depending on the counting rate but is monitored continuously with scalers. The systematic error on this computer dead time is much smaller than 0.3%.
- For solid targets, the thickness of the target can be measured within 0.5%. With ^{4}He gas target, in previous experiments, the thickness has been determined with an accuracy of $\sim$1%. To reduce the uncertainty on the target thickness for ^{4}He target, we plan to study the fluctuation of the target density due to the beam heating and correct for it.
- The beam current is measured with several, independent method in Hall-A and an accuracy of 0.3% has been achieved.
- The acceptance of the spectrometer is determined using a Monte-Carlo simulation for each spectrometer. Currently available simulation model gives 1.0% of systematic error point-to-point within the acceptance for a point target. For an extended target like ^{4}He, it will be about 1.5% using reduced acceptance cut. To minimize this uncertainty, some ^{12}C elastic data will be taken for the acceptance calibration purposes for each beam energy and spectrometer angle setting.[1]

[1]The uncertainty on the overall normalization is about 3% but would affect the R_L result only by the same amount (3%) since it changes cross sections at forward and backward angle by the same factor.

Source	Solid Target	Gas Target
Beam Energy (4×10^{-4})	<0.3	<0.3
Momentum reconstruction	<0.3	<0.3
Detector Inefficiency	<0.3	<0.3
Dead Time Corrections	<0.3	<0.3
Interpolation	<0.3	<0.3
Beam Current	<0.3	<0.3
Scattering Angle (0.2 mrad)	0.5	0.5
Background	0.5	0.5
Target Density (relative)	0.5	1.0
Radiative Corrections	1.0	1.0
Acceptance (relative)	1.0	1.5
Total	1.7	2.2

Table 2: Major contributions to the systematic uncertainty (in %).

In addition, there is another contribution from the radiative corrections which is discussed in the next section. From past experience, we expect 1% of systematic error from the radiative corrections.

Since we are doing a Rosenbluth separation of R_L and R_T, the uncertainty on the spectrometer angle or beam energy contributes to the systematic uncertainties on both response functions and the Coulomb Sum.

- The uncertainty of the spectrometer angle (0.7 mrad for Hall A spectrometers) has effects of 1 to 1.5 % on R_L. We plan to reduce this uncertainty to 0.2 mrad by taking calibration data at each angle.

- The uncertainty of the beam energy (2×10^{-4}) has effects of less than 0.3%

Finally, there is a systematic uncertainty from the interpolation of cross sections to constant $|\mathbf{q}|$ and we estimate it to be 0.5%. Table 2 summarizes all the major contributions to the systematic uncertainty.

By adding all the contributions in quadrature except that from the beam energy uncertainty, we can achieve a systematic error on the interpolated cross sections of 2.2% and 1.7% for ^{4}He gas target and solid targets, respectively. This means that the final systematic uncertainty on R_L will be

2.2 and 1.7 times the statistical uncertainty. Then the contribution from the scattering angle uncertainty (0.5%) should be added in quadrature. The final estimate of systematic uncertainties are plotted on Figures 7, 8 and 9.

8 Radiative Corrections

After removing all the backgrounds described above, the resulting cross sections need to be corrected for radiative effects. We will use the Mo and Tsai procedure without any energy or angular peaking approximations. Since we have taken enough spectra at various incident energies, we should be able to do reliable radiative corrections and achieve a systematic error less than 1%. Two target thicknesses will be used for ^{208}Pb to verify the external radiative corrections.

9 Coulomb Corrections for High Z Nucleus

Among the chosen targets, we expect the Coulomb corrections to be negligible for ^{4}He and ^{12}C. However, for high Z nucleus, such as ^{208}Pb, they can be significant. In the literature, two methods for performing the Coulomb corrections have been used: one used by Jourdan[24, 25] in his recent analysis which applied Coulomb corrections through LEMA (tested to be consistent with a full DWBA calculation by the Ohio group.[26]), the other known as standard EMA[34] used recently to describe successfully e^+ and e^- quasi-elastic scattering off ^{208}Pb[27].

In the EMA, the energies of the incident and scattered electron E and E' are replaced by $E_{\rm eff} = E - V_C$ and $E'_{\rm eff} = E' - V_C$, where V_C is the value of the effective Coulomb potential energy seen by the electron during the scattering process. The Rosenbluth formula can then be applied if we replace Q^2 and $\mathbf{q}^2$ by $Q^2_{\rm eff}$ and $\mathbf{q}^2_{\rm eff}$, respectively, while leaving the Mott cross section unchanged.[34] The values of V_C can be taken from Table II of Ref. [27].

At this time, LEMA does not reproduce the recent e^+/e^- quasi-elastic scattering data. However, the full DWBA calculation has not been checked against the same data and we expect this issue to be resolved in the near future.

To analyze our experiment, we will use whatever Coulomb correction method deemed to be correct and reliable.

10 Counting Rates and Required Time

To estimate the cross sections, we used the program by Lightbody and O'Connel. To evaluate the required time to do the measurement, we used a small solid angle of 4.4 msr for collimator solid angle of Hall-A spectrometer and $\pm$ 3.5% for the momentum acceptance. Beam current has been maintained under 50 μA. Also, the counting rate by the data acquisition system is limited to 2 kHz per spectrometer.

The number of counts per second is given by the following formula:

$$\text{event rate} = \frac{d^3\sigma}{d\Omega d\omega}\Delta\omega\Delta\Omega\frac{tN_A}{A}\frac{I}{e},$$

where

t is the target thickness (we used 100 mg/cm^2),
$N_A = 6.022 \times 10^{23}$ is the Avogadro number,
A is the mass number of the target nucleus,
I is the beam current, and e is the charge of the electron.

From these conditions, we have evaluated the necessary time to obtain statistical error of 1% per 10 MeV excitation energy bin. Table 4 shows estimated data acquisition time for each incident beam energy and spectrometer angle setting. Each line represents time required to take data on all four targets. Since we can use both spectrometers in Hall-A simultaneously to do measurements, the actual required time for data taking will be about 70% of the estimated time.[2]

All the overhead is summarized in Table 3. For the beam energy change, we assumed 1 shift for the change of number of passes and 2 shifts when it is necessary to fine-tune individual cavities. We have regrouped the beam energies as follows (all energies are in GeV).

$$(0.8, 1.6, 2.4, 3.2, 4.0), \quad (0.5, 1.0, 2.0), \quad (0.9, 3.6)$$
$$(0.7, 2.8), \quad (0.6, 1.2), \quad (1.1), \quad (0.4)$$

[2]The two spectrometers are not measuring the same configuration in general. At high energy and the most forward angle measurement, they can be at the same angle but at different momentum settings. For all the other energies, one spectrometer (A) will be at backward angle while the other (B) is at forward angle. In general, the forward angle measurements are short and spectrometer A can then move to a backward angle to minimize waste of time.

Item	Time (Hour)
Beam Energy Change	$21 \times 8 = 168$
Beam Energy Measurement	$16 \times 2 = 32$
Beam Current Calibration	$4 \times 1 = 4$
Spectrometer Acceptance Calibration Data	$28 \times 3/4 = 21$
Spectrometer Change (Angle & Momentum)	$286 \times 0.5 \times 0.7 = 100.1$
Target Change	$143 \times 5 \times 1/12 = 59.6$
Set-up and Test	$3 \times 24 = 72$
Total	456.7 (= 19 days)

Table 3: Estimation of the overhead

It takes one shift to change energies within the same group since we only need to change number of passes. However, it takes two shifts to change from one group to another. So, we need 9 changes in number of passes and 6 changes of LINAC energies, requiring a total of 21 shifts.

There are two methods to do beam energy measurements: ep and Arc measurements. We assigned one hour for each method. Beam current calibration requires one hour for each beam energy.

We would like to take some ^{12}C elastic data for spectrometer acceptance calibration for each beam energy and spectrometer angle. For this we need 1/2 hour to change the spectrometer configuration and another 15 minutes to take data.

There is a total of 286 different settings for spectrometer angle and momemtum and each change of setting requires 1/2 hour. Since we are using two spectrometers, we also expect that this overhead will be reduced by 30%.

A target change takes 5 minutes and there are 5 targets for each momentum setting (^{3}He, ^{12}C, ^{56}Fe and two different thicknesses for ^{206}Pb).

Finally, we need 3 days in the beginning for set-up and testing.

By adding the time for data taking and overhead, we reach 29 days of beam time for this measurement.

As mentioned in Section 6 on the important background issue, we need to study the electrons scattered inside the spectrometer to design an optimal collimator which reduces to negligible level or eliminates the effect. For this study, we also ask for a separate beam time of three days before the main experiment.

11 Summary

We propose to make a precision measurement of R_L and R_T of quasi-elastic electron scattering in the momentum transfer range 0.55 GeV/c $\leq |\mathbf{q}| \leq$ 1.0 GeV/c. The experiment will measure inclusive electron scattering cross section at various kinematic conditions (beam and scattered electron energy and scattering angle) on four nuclei: ^{4}He, ^{12}C, ^{56}Fe and ^{208}Pb. Using R_L, we will evaluate the Coulomb Sum and study its evolution in the momentum range mentioned above. This new measurement will shed light on nucleon properties in the nuclear medium for various nuclear densities.

To do this measurement, we ask for 29 days of beam time and three additional days before the main experiment to study backgrounds from the electrons scattered inside the spectrometer.

References

[1] M. Birse, J. Phys. **G20**, (1994) 1537.

[2] K.W. McVoy and L. Van Hove, Phys. Rev. **125**, (1962) 1034.

[3] T. de Forest, Jr., Nucl. Phys. **A414** (1984) 347.

[4] M. R. Frank, B. K. Jennings and G. A. Miller, Phys. Rev. C **54**, 920 (1996).

[5] R. Altemus *et al.,* Phys. Rev. Lett. **44**, 965 (1980).

[6] M. Deady *et al.,* Phys. Rev. C **28**, 631 (1983).

[7] A. Hotta *et al.,* Phys. Rev. C **30**, 87 (1984).

[8] M. Deady *et al.,* Phys. Rev. C **33**, 1897 (1986).

[9] C.C. Blatchley *et al.,* Phys. Rev. C **34**, 1243 (1986).

[10] S.A. Dytman *et al.,* Phys. Rev. C **38**, 800 (1988).

[11] T.C. Yates *et al.,* Phys. Lett. **312B**, 382 (1993).

[12] C. Williamson *et al.,* Phys. Rev. C **56**, 3152 (1997).

[13] P. Barreau *et al.,* Nucl. Phys. **A402**, 515 (1983).

[14] Z.-E. Meziani *et al.,* Phys. Rev. Lett. **52**, 2130 (1984).

[15] Z.-E. Meziani *et al.,* Phys. Rev. Lett. **54**, 1233 (1985).

[16] C. Marchand *et al.,* Phys. Lett. **153B**, 29 (1985).

[17] A. Zghiche *et al.,* Nucl. Phys. **A572**, 513 (1994).

[18] J. P. Chen *et al.,* Phys. Rev. Lett. **66**, 1283 (1991).

[19] Z.-E. Meziani *et al.,* Phys. Rev. Lett. **69**, 41 (1992).

[20] J. V. Noble, Phys. Rev. Lett. **46**, 412 (1981).

[21] L. S. Celenza *et al.,* Phys. Rev. Lett. **53**, 891 (1984).

[22] P. J. Mulders, Nucl. Phys. A **459**, 525 (1986).

[23] G.E. Brown and M. Rho, Phys. Lett. **222B**, 324 (1989).

[24] J. Jourdan, Phys. Lett. **353B**, 189 (1995).

[25] J. Jourdan, Nucl. Phys. **A603**, 117 (1996).

[26] D. Onley, Y. Yin and L. E. Wright, Phys. Rev. C **45**, 1333 (1992); K. S. Kim, L.E. Wright, Y. Yin and D. W. Kosik, Phys. Rev. C **54**, 2515 (1996).

[27] P. Gueye *et al.,* Phys. Rev. C **60**, 044308 (1999).

[28] J. Morgenstern and Z.-E. Meziani, submitted to Phys. Rev. Lett. and private communication.

[29] G.G. Simon *et al.,* Nucl. Phys. A **333**, 381 (1980).

[30] C. Herberg *et al.,* Eur. Phys. **A5**, 131 (1999).

[31] A. Fabrocini and S. Fantoni, Nucl. Phys. A **503**, 375 (1989).

[32] R. Schiavilla *et al.,* Nucl. Phys. A **499**, 301 (1989).

[33] D. T. Baran *et al.,* Phys. Rev. Lett. **61**, 400 (1988).

[34] R. Rosenfelder, Ann. Phys., **128**, (1980).

E_{beam}	θ	No. of P_{ref}	Time (Hour)	Sub-Total (Hour)
400.0	90.0°	17	11.3	
	120.0°	16	10.9	22.3
500.0	90.0°	20	13.9	
	120.0°	18	16.1	30.0
600.0	60.0°	16	10.7	
	90.0°	17	15.6	
	120.0°	18	22.7	48.9
700.0	60.0°	13	8.8	
	90.0°	14	20.6	
	120.0°	15	28.2	57.6
800.0	60.0°	11	8.5	
	90.0°	13	23.1	
	120.0°	13	22.0	53.7
900.0	60.0°	10	10.7	
	90.0°	12	24.3	
	120.0°	6	13.8	48.8
1000.0	60.0°	9	15.3	
	90.0°	6	11.4	26.8
1100.0	60.0°	9	18.4	18.4
1200.0	15.0°	6	4.0	
	60.0°	8	20.2	24.2
1600.0	15.0°	4	2.7	2.7
2000.0	15.0°	3	2.0	2.0
2400.0	15.0°	3	2.0	2.0
2800.0	15.0°	3	2.0	2.0
3200.0	15.0°	3	2.2	2.2
3600.0	15.0°	2	1.8	1.8
4000.0	15.0°	1	2.1	2.1
Total Time (hours)				345.2
With 2 Spectrometers				241.6

Table 4: Estimation of the required time at each beam energy

E_{beam} (MeV)	θ	P_{ref} (MeV/c)	Q^2 (GeV^2)	ω (MeV)	W (GeV/c^2)
400.0	90.0°	103.895	0.0831	296.11	1.1650
400.0	90.0°	111.431	0.0891	288.57	1.1563
400.0	90.0°	119.514	0.0956	280.49	1.1469
400.0	90.0°	128.184	0.1025	271.82	1.1367
400.0	90.0°	137.482	0.1100	262.52	1.1257
400.0	90.0°	147.455	0.1180	252.54	1.1137
400.0	90.0°	158.151	0.1265	241.85	1.1008
400.0	90.0°	169.623	0.1357	230.38	1.0867
400.0	90.0°	181.927	0.1455	218.07	1.0715
400.0	90.0°	195.124	0.1561	204.88	1.0548
400.0	90.0°	209.278	0.1674	190.72	1.0367
400.0	90.0°	224.459	0.1796	175.54	1.0169
400.0	90.0°	240.741	0.1926	159.26	0.9952
400.0	90.0°	258.204	0.2066	141.80	0.9714
400.0	90.0°	276.934	0.2215	123.07	0.9452
400.0	90.0°	297.023	0.2376	102.98	0.9163
400.0	90.0°	318.568	0.2549	81.43	0.8842
400.0	120.0°	102.432	0.1229	297.57	1.1490
400.0	120.0°	109.863	0.1318	290.14	1.1390
400.0	120.0°	117.832	0.1414	282.17	1.1281
400.0	120.0°	126.379	0.1517	273.62	1.1164
400.0	120.0°	135.547	0.1627	264.45	1.1037
400.0	120.0°	145.379	0.1745	254.62	1.0899
400.0	120.0°	155.925	0.1871	244.07	1.0749
400.0	120.0°	167.235	0.2007	232.76	1.0585
400.0	120.0°	179.366	0.2152	220.63	1.0407
400.0	120.0°	192.377	0.2309	207.62	1.0213
400.0	120.0°	206.332	0.2476	193.67	1.0000
400.0	120.0°	221.299	0.2656	178.70	0.9767
400.0	120.0°	237.352	0.2848	162.65	0.9511
400.0	120.0°	254.569	0.3055	145.43	0.9228
400.0	120.0°	273.036	0.3276	126.96	0.8914

Table 5: Table of Kinematics

E_{beam} (MeV)	θ	P_{ref} (MeV/c)	Q^2 (GeV^2)	ω (MeV)	W (GeV/c^2)
400.0	120.0°	292.841	0.3514	107.16	0.8565
500.0	90.0°	100.831	0.1008	399.17	1.2382
500.0	90.0°	108.145	0.1081	391.86	1.2297
500.0	90.0°	115.990	0.1160	384.01	1.2205
500.0	90.0°	124.404	0.1244	375.60	1.2105
500.0	90.0°	133.428	0.1334	366.57	1.1997
500.0	90.0°	143.107	0.1431	356.89	1.1880
500.0	90.0°	153.488	0.1535	346.51	1.1754
500.0	90.0°	164.621	0.1646	335.38	1.1617
500.0	90.0°	176.563	0.1766	323.44	1.1468
500.0	90.0°	189.370	0.1894	310.63	1.1306
500.0	90.0°	203.107	0.2031	296.89	1.1129
500.0	90.0°	217.840	0.2178	282.16	1.0937
500.0	90.0°	233.642	0.2336	266.36	1.0727
500.0	90.0°	250.590	0.2506	249.41	1.0497
500.0	90.0°	268.768	0.2688	231.23	1.0245
500.0	90.0°	288.264	0.2883	211.74	0.9967
500.0	90.0°	309.174	0.3092	190.83	0.9660
500.0	90.0°	331.602	0.3316	168.40	0.9320
500.0	90.0°	355.655	0.3557	144.35	0.8940
500.0	90.0°	381.454	0.3815	118.55	0.8515
500.0	120.0°	104.950	0.1574	395.05	1.2120
500.0	120.0°	112.563	0.1688	387.44	1.2013
500.0	120.0°	120.728	0.1811	379.27	1.1898
500.0	120.0°	129.486	0.1942	370.51	1.1773
500.0	120.0°	138.878	0.2083	361.12	1.1637
500.0	120.0°	148.952	0.2234	351.05	1.1490
500.0	120.0°	159.757	0.2396	340.24	1.1330
500.0	120.0°	171.346	0.2570	328.65	1.1155
500.0	120.0°	183.775	0.2757	316.23	1.0966
500.0	120.0°	197.106	0.2957	302.89	1.0758
500.0	120.0°	211.404	0.3171	288.60	1.0531

Table 6: Table of Kinematics (Continued)

E_{beam} (MeV)	θ	P_{ref} (MeV/c)	Q^2 (GeV^2)	ω (MeV)	W (GeV/c^2)
500.0	120.0°	226.739	0.3401	273.26	1.0282
500.0	120.0°	243.186	0.3648	256.81	1.0008
500.0	120.0°	260.826	0.3912	239.17	0.9706
500.0	120.0°	279.747	0.4196	220.25	0.9370
500.0	120.0°	300.039	0.4501	199.96	0.8997
500.0	120.0°	321.803	0.4827	178.20	0.8578
500.0	120.0°	345.147	0.5177	154.85	0.8106
600.0	60.0°	174.826	0.1049	425.17	1.2562
600.0	60.0°	187.508	0.1125	412.49	1.2436
600.0	60.0°	201.110	0.1207	398.89	1.2300
600.0	60.0°	215.698	0.1294	384.30	1.2152
600.0	60.0°	231.344	0.1388	368.66	1.1991
600.0	60.0°	248.126	0.1489	351.87	1.1816
600.0	60.0°	266.125	0.1597	333.87	1.1626
600.0	60.0°	285.429	0.1713	314.57	1.1418
600.0	60.0°	306.134	0.1837	293.87	1.1191
600.0	60.0°	328.340	0.1970	271.66	1.0942
600.0	60.0°	352.158	0.2113	247.84	1.0669
600.0	60.0°	377.703	0.2266	222.30	1.0368
600.0	60.0°	405.101	0.2431	194.90	1.0035
600.0	60.0°	434.486	0.2607	165.51	0.9665
600.0	60.0°	466.004	0.2796	134.00	0.9252
600.0	60.0°	499.807	0.2999	100.19	0.8787
600.0	90.0°	143.257	0.1719	456.74	1.2531
600.0	90.0°	153.648	0.1844	446.35	1.2403
600.0	90.0°	164.794	0.1978	435.21	1.2264
600.0	90.0°	176.748	0.2121	423.25	1.2113
600.0	90.0°	189.569	0.2275	410.43	1.1949
600.0	90.0°	203.320	0.2440	396.68	1.1770
600.0	90.0°	218.069	0.2617	381.93	1.1576
600.0	90.0°	233.887	0.2807	366.11	1.1363
600.0	90.0°	250.853	0.3010	349.15	1.1131

Table 7: Table of Kinematics (Continued)

E_{beam} (MeV)	θ	P_{ref} (MeV/c)	Q^2 (GeV^2)	ω (MeV)	W (GeV/c^2)
600.0	90.0°	269.050	0.3229	330.95	1.0876
600.0	90.0°	288.566	0.3463	311.43	1.0596
600.0	90.0°	309.499	0.3714	290.50	1.0288
600.0	90.0°	331.949	0.3983	268.05	0.9946
600.0	90.0°	356.028	0.4272	243.97	0.9566
600.0	90.0°	381.854	0.4582	218.15	0.9141
600.0	90.0°	409.553	0.4915	190.45	0.8661
600.0	90.0°	439.262	0.5271	160.74	0.8116
600.0	120.0°	119.136	0.2144	480.86	1.2543
600.0	120.0°	127.778	0.2300	472.22	1.2415
600.0	120.0°	137.047	0.2467	462.95	1.2277
600.0	120.0°	146.988	0.2646	453.01	1.2127
600.0	120.0°	157.651	0.2838	442.35	1.1964
600.0	120.0°	169.086	0.3044	430.91	1.1787
600.0	120.0°	181.352	0.3264	418.65	1.1594
600.0	120.0°	194.507	0.3501	405.49	1.1383
600.0	120.0°	208.616	0.3755	391.38	1.1153
600.0	120.0°	223.749	0.4027	376.25	1.0900
600.0	120.0°	239.979	0.4320	360.02	1.0623
600.0	120.0°	257.387	0.4633	342.61	1.0317
600.0	120.0°	276.058	0.4969	323.94	0.9979
600.0	120.0°	296.083	0.5329	303.92	0.9602
600.0	120.0°	317.560	0.5716	282.44	0.9181
600.0	120.0°	340.596	0.6131	259.40	0.8708
600.0	120.0°	365.302	0.6575	234.70	0.8169
600.0	120.0°	391.801	0.7052	208.20	0.7548
700.0	60.0°	245.996	0.1722	454.00	1.2510
700.0	60.0°	263.841	0.1847	436.16	1.2324
700.0	60.0°	282.979	0.1981	417.02	1.2122
700.0	60.0°	303.506	0.2125	396.49	1.1902
700.0	60.0°	325.522	0.2279	374.48	1.1661
700.0	60.0°	349.135	0.2444	350.87	1.1397

Table 8: Table of Kinematics (Continued)

E_{beam} (MeV)	θ	P_{ref} (MeV/c)	Q^2 (GeV^2)	ω (MeV)	W (GeV/c^2)
700.0	60.0°	374.461	0.2621	325.54	1.1106
700.0	60.0°	401.624	0.2811	298.38	1.0786
700.0	60.0°	430.758	0.3015	269.24	1.0432
700.0	60.0°	462.004	0.3234	238.00	1.0038
700.0	60.0°	495.518	0.3469	204.48	0.9598
700.0	60.0°	531.462	0.3720	168.54	0.9102
700.0	60.0°	570.014	0.3990	129.99	0.8538
700.0	90.0°	198.203	0.2775	501.80	1.2448
700.0	90.0°	212.580	0.2976	487.42	1.2257
700.0	90.0°	228.000	0.3192	472.00	1.2049
700.0	90.0°	244.539	0.3424	455.46	1.1822
700.0	90.0°	262.278	0.3672	437.72	1.1573
700.0	90.0°	281.303	0.3938	418.70	1.1300
700.0	90.0°	301.709	0.4224	398.29	1.1000
700.0	90.0°	323.594	0.4530	376.41	1.0669
700.0	90.0°	347.067	0.4859	352.93	1.0302
700.0	90.0°	372.243	0.5211	327.76	0.9893
700.0	90.0°	399.245	0.5589	300.75	0.9434
700.0	90.0°	428.206	0.5995	271.79	0.8917
700.0	90.0°	459.268	0.6430	240.73	0.8326
700.0	90.0°	492.582	0.6896	207.42	0.7642
700.0	120.0°	162.697	0.3417	537.30	1.2458
700.0	120.0°	174.499	0.3664	525.50	1.2268
700.0	120.0°	187.157	0.3930	512.84	1.2061
700.0	120.0°	200.733	0.4215	499.27	1.1835
700.0	120.0°	215.294	0.4521	484.71	1.1588
700.0	120.0°	230.911	0.4849	469.09	1.1316
700.0	120.0°	247.661	0.5201	452.34	1.1018
700.0	120.0°	265.626	0.5578	434.37	1.0688
700.0	120.0°	284.894	0.5983	415.11	1.0323
700.0	120.0°	305.560	0.6417	394.44	0.9917
700.0	120.0°	327.725	0.6882	372.27	0.9462

Table 9: Table of Kinematics (Continued)

E_{beam} (MeV)	θ	P_{ref} (MeV/c)	Q^2 (GeV^2)	ω (MeV)	W (GeV/c^2)
700.0	120.0°	351.498	0.7381	348.50	0.8948
700.0	120.0°	376.995	0.7917	323.00	0.8362
700.0	120.0°	404.342	0.8491	295.66	0.7683
700.0	120.0°	433.672	0.9107	266.33	0.6882
800.0	60.0°	316.302	0.2530	483.70	1.2409
800.0	60.0°	339.246	0.2714	460.75	1.2159
800.0	60.0°	363.855	0.2911	436.14	1.1885
800.0	60.0°	390.248	0.3122	409.75	1.1583
800.0	60.0°	418.557	0.3348	381.44	1.1251
800.0	60.0°	448.918	0.3591	351.08	1.0883
800.0	60.0°	481.482	0.3852	318.52	1.0475
800.0	60.0°	516.408	0.4131	283.59	1.0018
800.0	60.0°	553.868	0.4431	246.13	0.9504
800.0	60.0°	594.045	0.4752	205.96	0.8919
800.0	60.0°	637.136	0.5097	162.86	0.8247
800.0	90.0°	233.872	0.3742	566.13	1.2545
800.0	90.0°	250.836	0.4013	549.16	1.2307
800.0	90.0°	269.032	0.4305	530.97	1.2047
800.0	90.0°	288.547	0.4617	511.45	1.1762
800.0	90.0°	309.478	0.4952	490.52	1.1448
800.0	90.0°	331.927	0.5311	468.07	1.1102
800.0	90.0°	356.005	0.5696	444.00	1.0718
800.0	90.0°	381.829	0.6109	418.17	1.0290
800.0	90.0°	409.526	0.6552	390.47	0.9810
800.0	90.0°	439.233	0.7028	360.77	0.9269
800.0	90.0°	471.094	0.7538	328.91	0.8650
800.0	90.0°	505.267	0.8084	294.73	0.7933
800.0	90.0°	541.919	0.8671	258.08	0.7083
800.0	120.0°	189.704	0.4553	610.30	1.2553
800.0	120.0°	203.465	0.4883	596.53	1.2316
800.0	120.0°	218.224	0.5237	581.78	1.2057
800.0	120.0°	234.053	0.5617	565.95	1.1772

Table 10: Table of Kinematics (Continued)

E_{beam} (MeV)	θ	P_{ref} (MeV/c)	Q^2 (GeV^2)	ω (MeV)	W (GeV/c^2)
800.0	120.0°	251.031	0.6025	548.97	1.1459
800.0	120.0°	269.241	0.6462	530.76	1.1114
800.0	120.0°	288.771	0.6931	511.23	1.0732
800.0	120.0°	309.718	0.7433	490.28	1.0305
800.0	120.0°	332.185	0.7972	467.81	0.9828
800.0	120.0°	356.281	0.8551	443.72	0.9288
800.0	120.0°	382.126	0.9171	417.87	0.8672
800.0	120.0°	409.845	0.9836	390.15	0.7959
800.0	120.0°	439.574	1.0550	360.43	0.7115
900.0	60.0°	373.450	0.3361	526.55	1.2399
900.0	60.0°	400.539	0.3605	499.46	1.2092
900.0	60.0°	429.594	0.3866	470.41	1.1753
900.0	60.0°	460.756	0.4147	439.24	1.1378
900.0	60.0°	494.179	0.4448	405.82	1.0963
900.0	60.0°	530.026	0.4770	369.97	1.0498
900.0	60.0°	568.474	0.5116	331.53	0.9976
900.0	60.0°	609.710	0.5487	290.29	0.9384
900.0	60.0°	653.938	0.5885	246.06	0.8704
900.0	60.0°	701.374	0.6312	198.63	0.7911
900.0	90.0°	272.028	0.4897	627.97	1.2548
900.0	90.0°	291.760	0.5252	608.24	1.2255
900.0	90.0°	312.924	0.5633	587.08	1.1933
900.0	90.0°	335.623	0.6041	564.38	1.1578
900.0	90.0°	359.969	0.6479	540.03	1.1184
900.0	90.0°	386.081	0.6949	513.92	1.0746
900.0	90.0°	414.087	0.7454	485.91	1.0256
900.0	90.0°	444.124	0.7994	455.88	0.9702
900.0	90.0°	476.340	0.8574	423.66	0.9070
900.0	90.0°	510.893	0.9196	389.11	0.8340
900.0	90.0°	547.953	0.9863	352.05	0.7478
900.0	90.0°	587.701	1.0579	312.30	0.6425
900.0	120.0°	218.256	0.5893	681.74	1.2554

Table 11: Table of Kinematics (Continued)

E_{beam} (MeV)	θ	P_{ref} (MeV/c)	Q^2 (GeV^2)	ω (MeV)	W (GeV/c^2)
900.0	120.0°	234.088	0.6320	665.91	1.2262
900.0	120.0°	251.069	0.6779	648.93	1.1940
900.0	120.0°	269.281	0.7271	630.72	1.1586
900.0	120.0°	288.815	0.7798	611.18	1.1193
900.0	120.0°	309.765	0.8364	590.24	1.0756
1000.0	60.0°	435.681	0.4357	564.32	1.2283
1000.0	60.0°	467.284	0.4673	532.72	1.1907
1000.0	60.0°	501.181	0.5012	498.82	1.1490
1000.0	60.0°	537.536	0.5375	462.46	1.1025
1000.0	60.0°	576.528	0.5765	423.47	1.0503
1000.0	60.0°	618.349	0.6183	381.65	0.9913
1000.0	60.0°	663.203	0.6632	336.80	0.9239
1000.0	60.0°	711.311	0.7113	288.69	0.8456
1000.0	60.0°	762.909	0.7629	237.09	0.7526
1000.0	90.0°	312.908	0.6258	687.09	1.2448
1000.0	90.0°	335.606	0.6712	664.39	1.2089
1000.0	90.0°	359.951	0.7199	640.05	1.1692
1000.0	90.0°	386.061	0.7721	613.94	1.1250
1000.0	90.0°	414.066	0.8281	585.93	1.0757
1000.0	90.0°	444.101	0.8882	555.90	1.0200
1100.0	60.0°	469.374	0.5163	630.63	1.2461
1100.0	60.0°	503.421	0.5538	596.58	1.2047
1100.0	60.0°	539.939	0.5939	560.06	1.1587
1100.0	60.0°	579.106	0.6370	520.89	1.1072
1100.0	60.0°	621.113	0.6832	478.89	1.0491
1100.0	60.0°	666.168	0.7328	433.83	0.9831
1100.0	60.0°	714.491	0.7859	385.51	0.9069
1100.0	60.0°	766.320	0.8430	333.68	0.8173
1100.0	60.0°	821.908	0.9041	278.09	0.7087
1200.0	15.0°	799.492	0.0654	400.51	1.2535
1200.0	15.0°	857.487	0.0701	342.51	1.2072
1200.0	15.0°	919.688	0.0752	280.31	1.1556

Table 12: Table of Kinematics (Continued)

E_{beam} (MeV)	θ	P_{ref} (MeV/c)	Q^2 (GeV^2)	ω (MeV)	W (GeV/c^2)
1200.0	15.0°	986.401	0.0807	213.60	1.0975
1200.0	15.0°	1057.953	0.0865	142.05	1.0316
1200.0	15.0°	1134.696	0.0928	65.30	0.9558
1200.0	60.0°	538.099	0.6457	661.90	1.2175
1200.0	60.0°	577.132	0.6926	622.87	1.1671
1200.0	60.0°	618.997	0.7428	581.00	1.1104
1200.0	60.0°	663.898	0.7967	536.10	1.0463
1200.0	60.0°	712.057	0.8545	487.94	0.9729
1200.0	60.0°	763.708	0.9164	436.29	0.8873
1200.0	60.0°	819.107	0.9829	380.89	0.7853
1200.0	60.0°	878.524	1.0542	321.48	0.6586
1600.0	15.0°	1217.595	0.1328	382.40	1.2123
1600.0	15.0°	1305.918	0.1424	294.08	1.1376
1600.0	15.0°	1400.648	0.1527	199.35	1.0515
1600.0	15.0°	1502.249	0.1638	97.75	0.9506
2000.0	15.0°	1620.957	0.2209	379.04	1.1727
2000.0	15.0°	1738.539	0.2370	261.46	1.0669
2000.0	15.0°	1864.651	0.2541	135.35	0.9402
2400.0	15.0°	1931.610	0.3159	468.39	1.2034
2400.0	15.0°	2071.727	0.3388	328.27	1.0779
2400.0	15.0°	2222.008	0.3634	177.99	0.9246
2800.0	15.0°	2237.969	0.4270	562.03	1.2301
2800.0	15.0°	2400.309	0.4580	399.69	1.0849
2800.0	15.0°	2574.425	0.4912	225.57	0.9036
3200.0	15.0°	2540.122	0.5539	659.88	1.2531
3200.0	15.0°	2724.380	0.5941	475.62	1.0880
3200.0	15.0°	2922.003	0.6372	278.00	0.8769
3600.0	15.0°	3044.032	0.7468	555.97	1.0872
3600.0	15.0°	3264.843	0.8010	335.16	0.8442
4000.0	15.0°	3603.040	0.9822	396.96	0.8048

Table 13: Table of Kinematics (Continued)

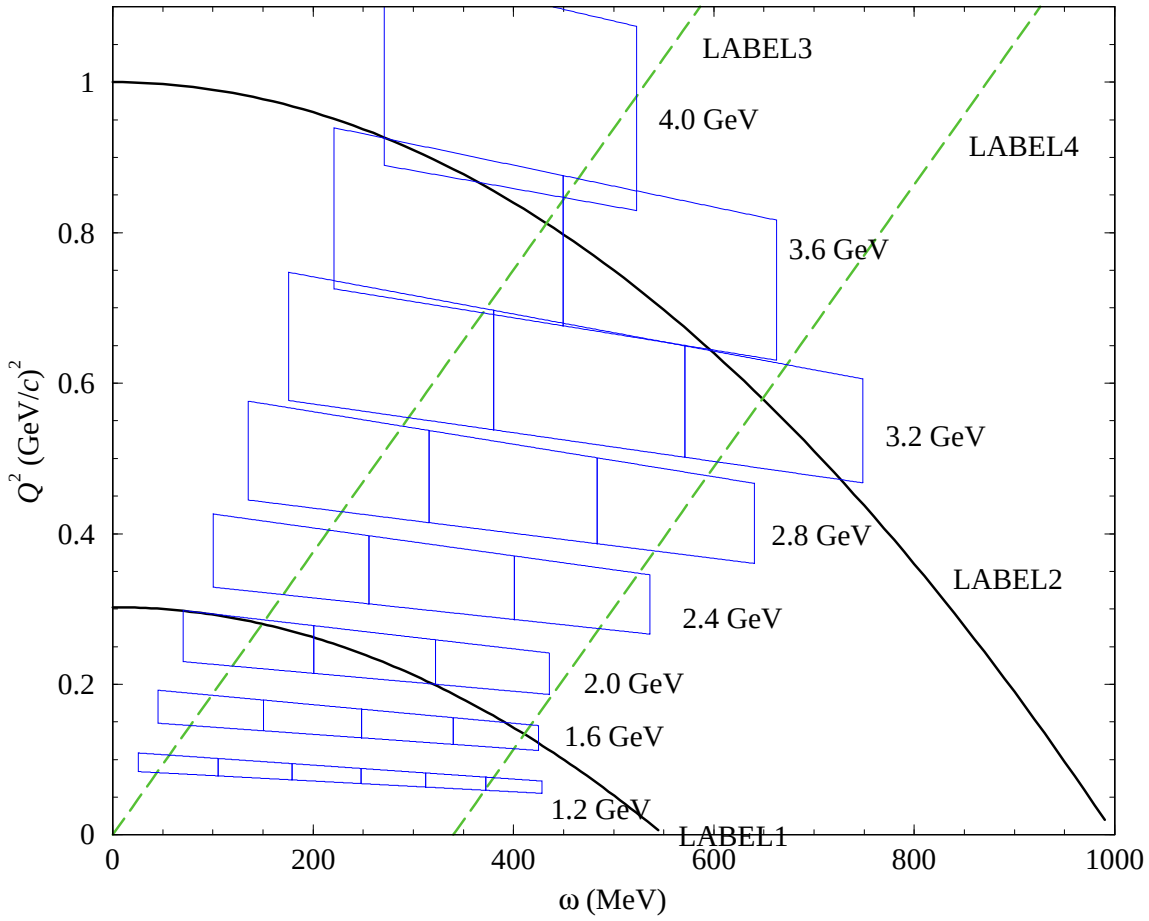

Figure 2: Kinematic coverage at 15°. The two solid lines correspond to $|\mathbf{q}| = 550$ MeV/c(lower one) and 1000 MeV/c (upper one). The two dashed lines correspond to $W = 940$ MeV/c^2 (left, quasi-elastic peak) and 1232 MeV/c^2 (right, Δ resonance). Each box represents the actual acceptance of the spectrometer at each individual momentum setting. Corresponding beam energies are also specified.

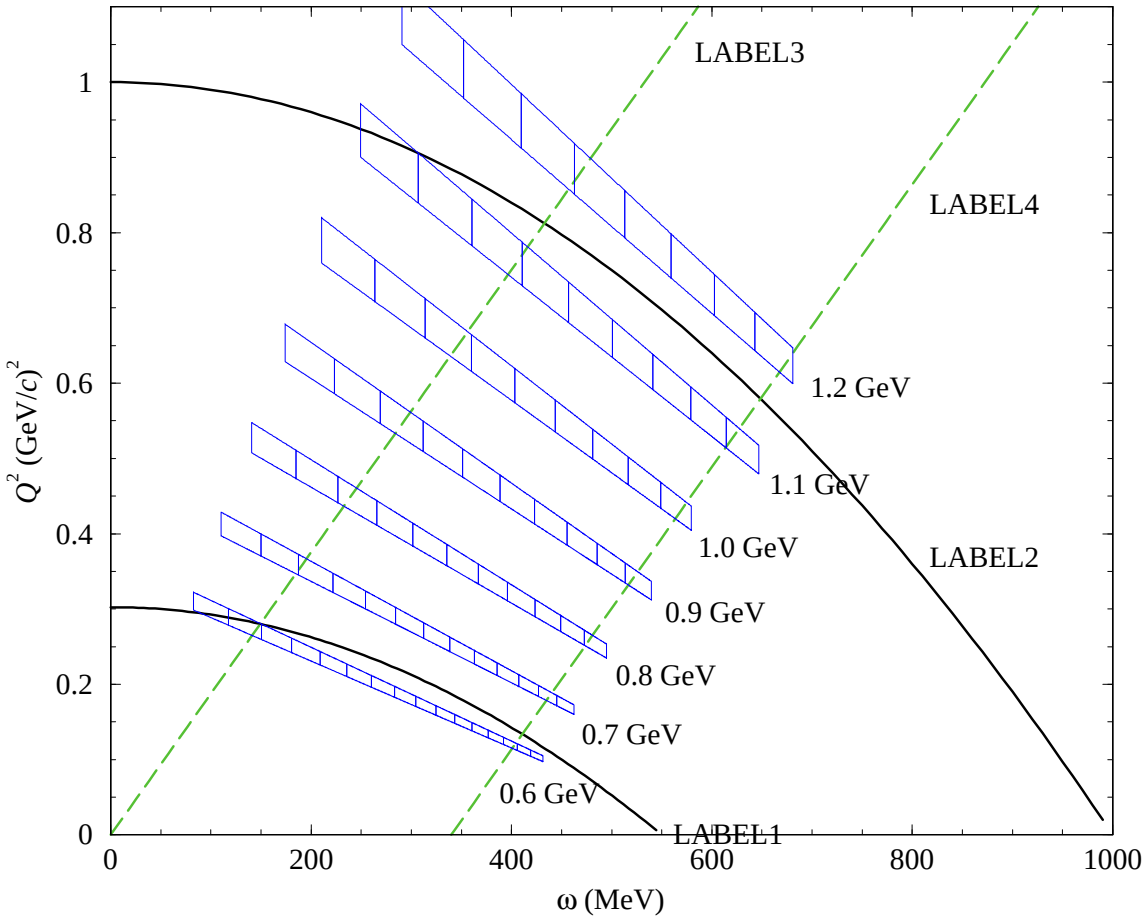

Figure 3: Kinematic coverage at 60°. The two solid lines correspond to $|\mathbf{q}| = 550$ MeV/c(lower one) and 1000 MeV/c (upper one). The two dashed lines correspond to $W = 940$ MeV/c^2 (left, quasi-elastic peak) and 1232 MeV/c^2 (right, Δ resonance). Each box represents the actual acceptance of the spectrometer at each individual momentum setting. Corresponding beam energies are also specified.

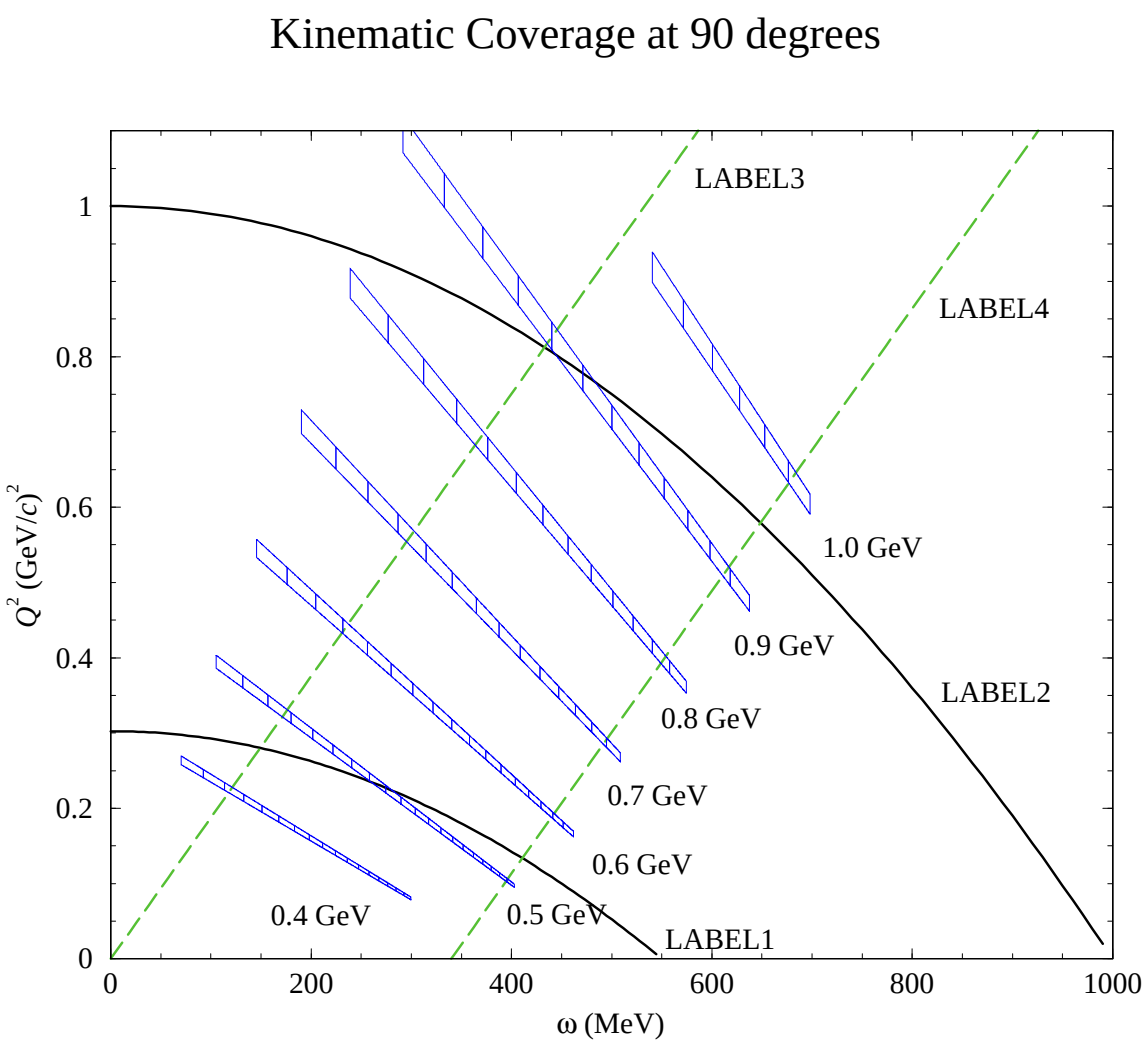

Figure 4: Kinematic coverage at 90°. The two solid lines correspond to $|\mathbf{q}| = 550$ MeV/c(lower one) and 1000 MeV/c (upper one). The two dashed lines correspond to $W = 940$ MeV/c^2 (left, quasi-elastic peak) and 1232 MeV/c^2 (right, Δ resonance). Each box represents the actual acceptance of the spectrometer at each individual momentum setting. Corresponding beam energies are also specified.

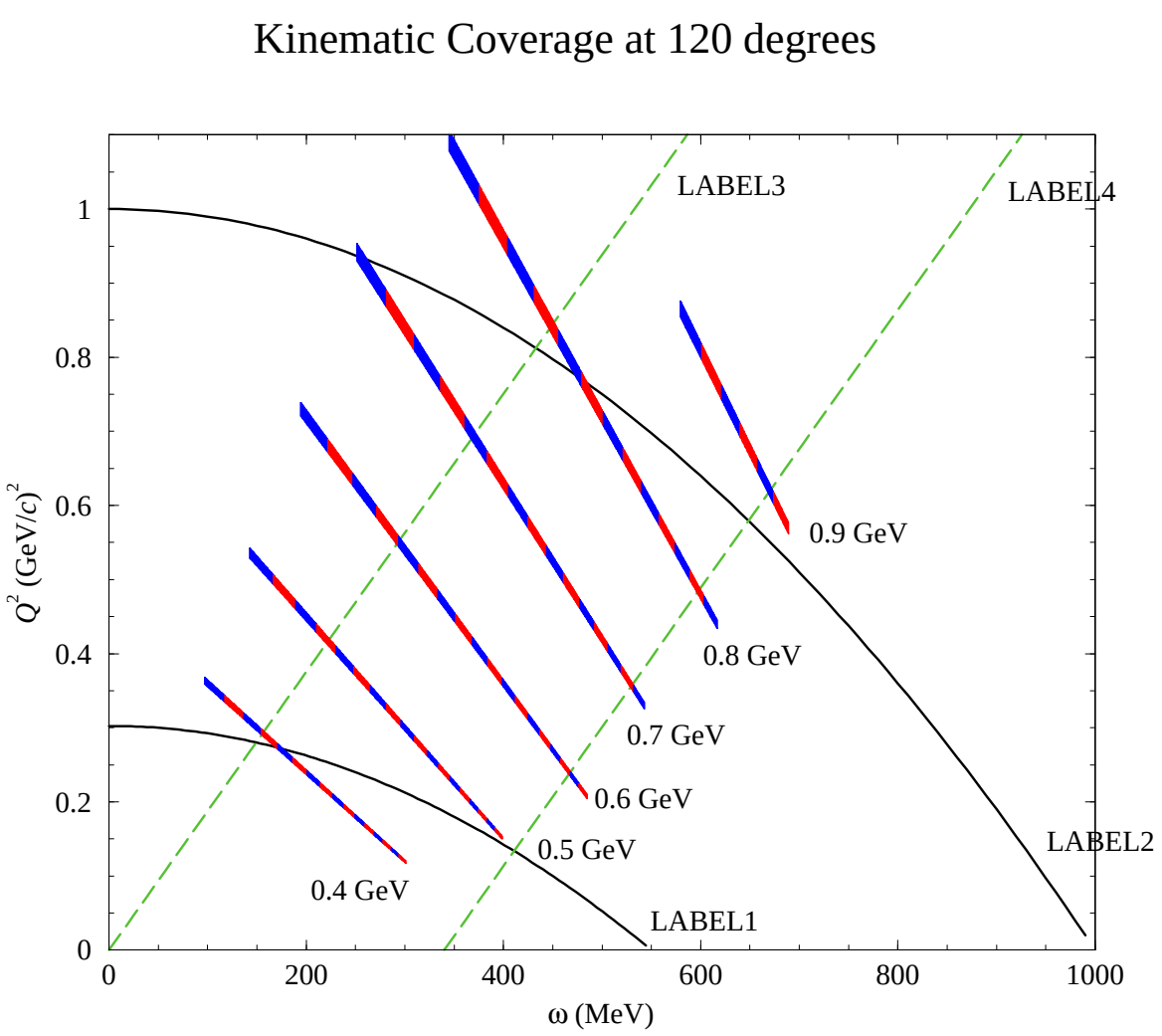

Figure 5: Kinematic coverage at 120°. The two solid lines correspond to $|\mathbf{q}| = 550$ MeV/c(lower one) and 1000 MeV/c (upper one). The two dashed lines correspond to $W = 940$ MeV/c^2 (left, quasi-elastic peak) and 1232 MeV/c^2 (right, Δ resonance). Each box represents the actual acceptance of the spectrometer at each individual momentum setting. Corresponding beam energies are also specified.

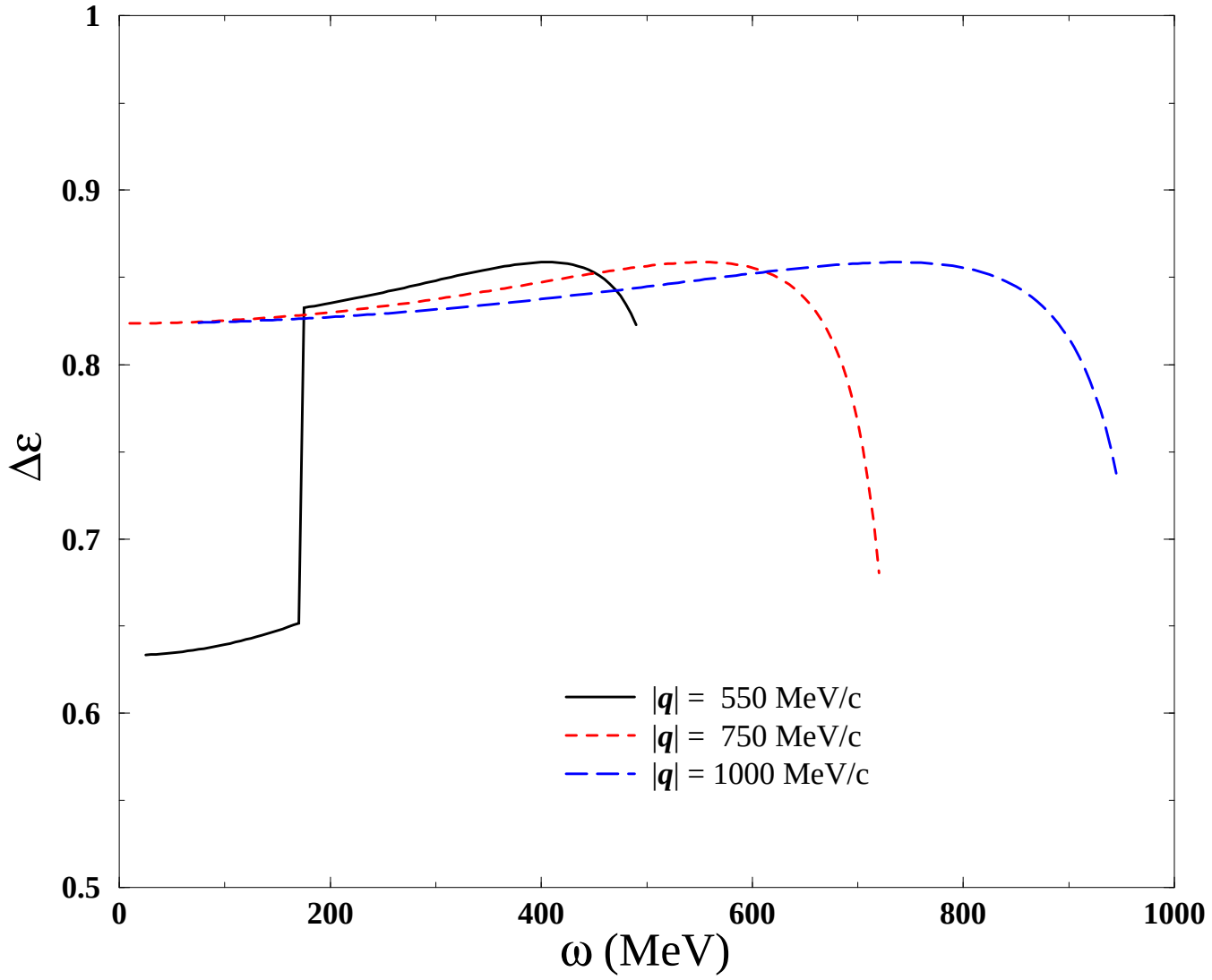

Figure 6: $\Delta\varepsilon$ achievable at Jefferson Lab for three values of $|\mathbf{q}|$.

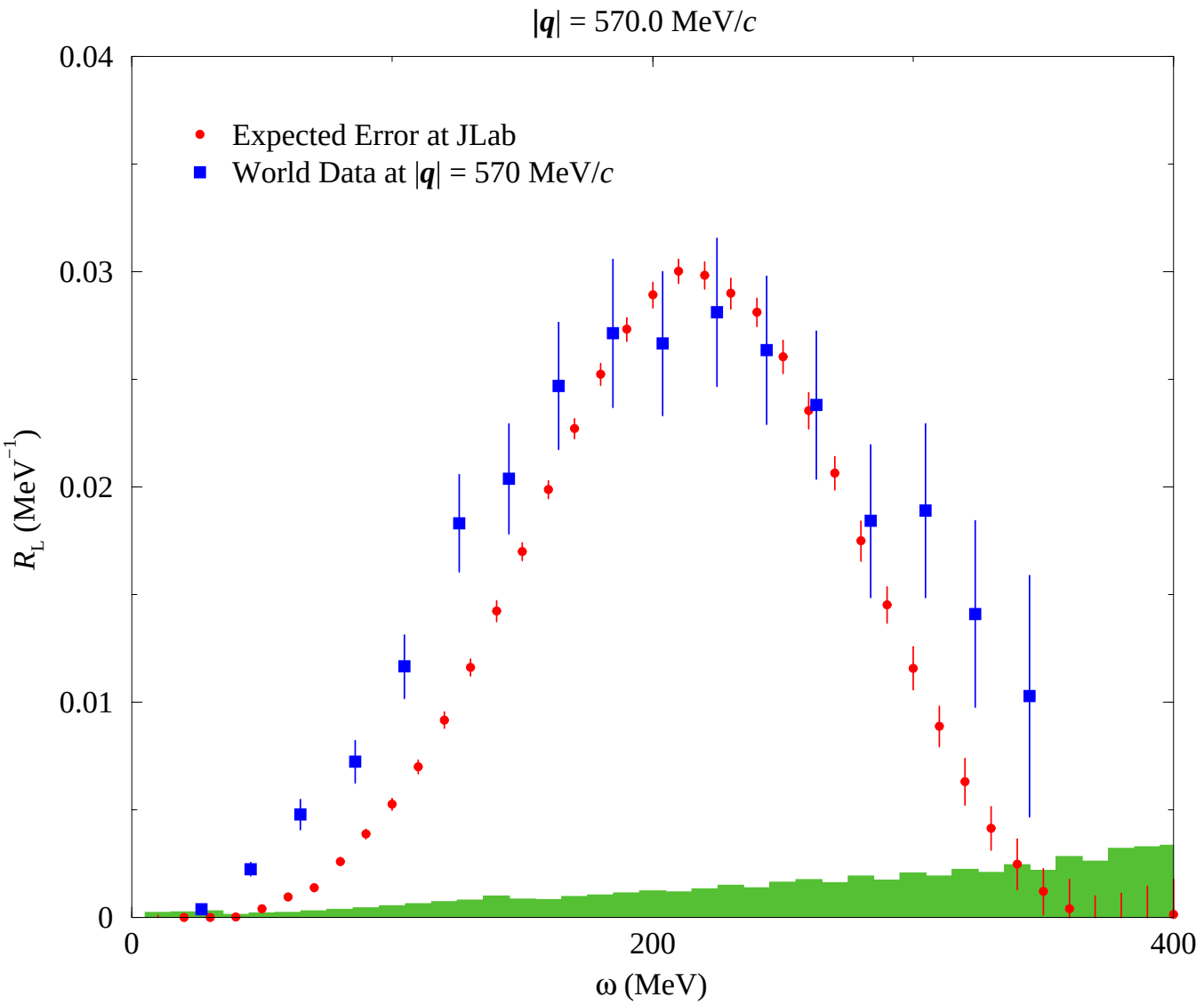

Figure 7: Comparison of expected statistical uncertainty on R_L from Jefferson Lab with the world data at $|\mathbf{q}| = 570$ MeV/c. The error bars for the world data are statistical only. The band at the horizontal axis represents estimated systematic uncertainties.

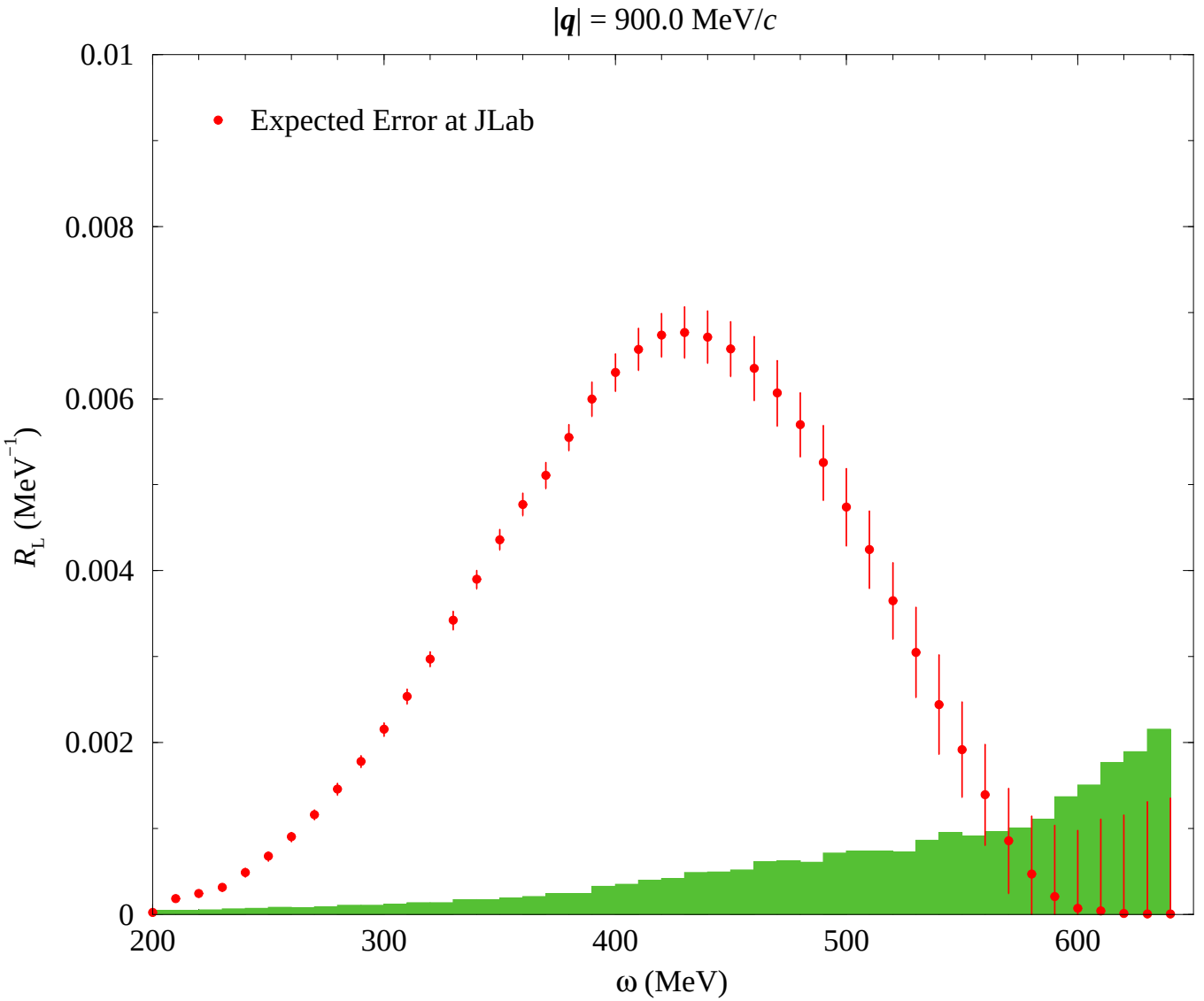

Figure 8: Expected statistical uncertainty on R_L from Jefferson Lab at $|\mathbf{q}| = 900$ MeV/c. The band at the horizontal axis represents estimated systematic uncertainties.

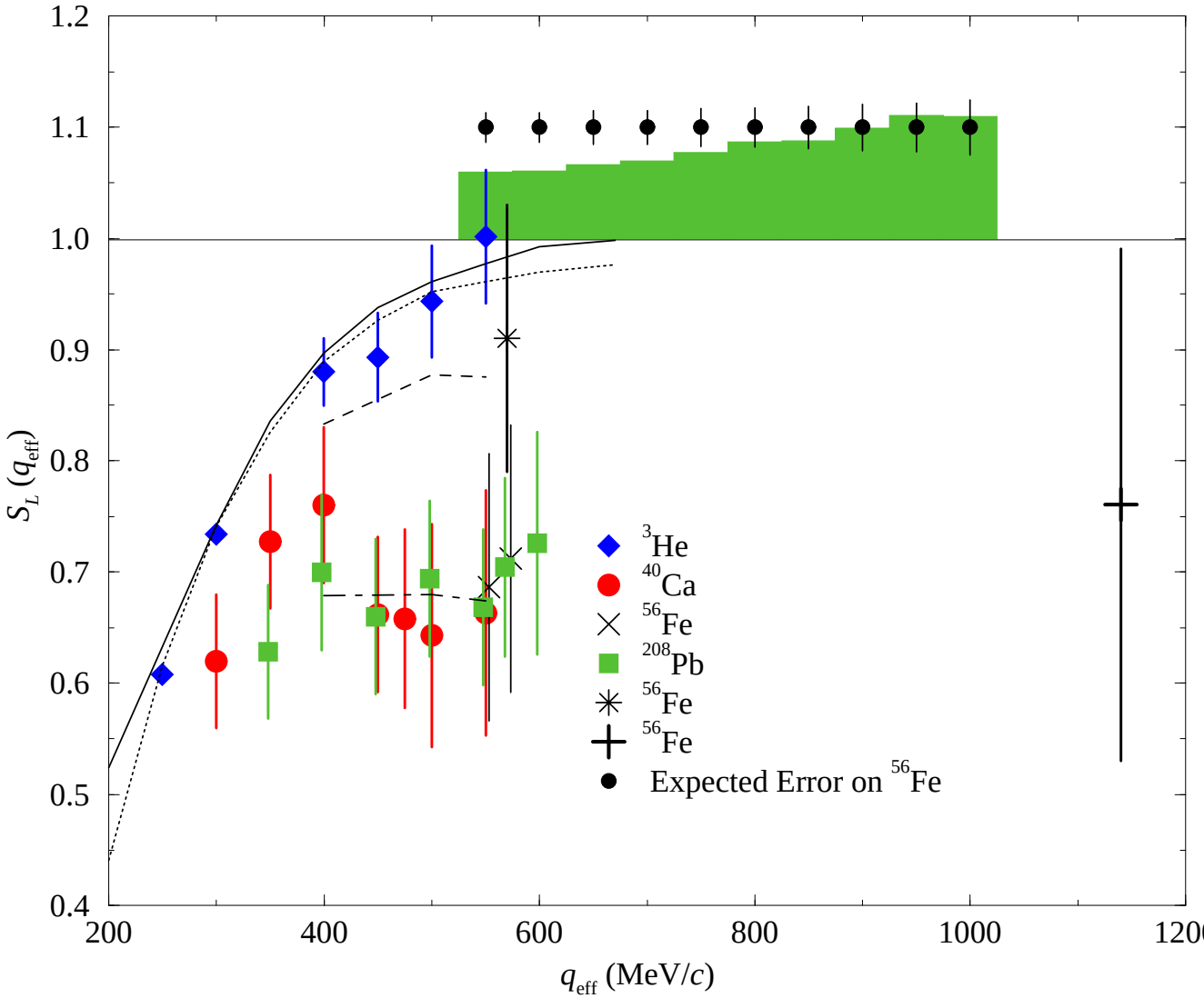

Figure 9: Comparison of expected statistical uncertainty on the Coulomb Sum from Jefferson Lab with the world data. Horizontal band represents estimated systematic uncertainties.